Contrib Mineral Petrol (2006) 151: 480–492
DOI 10.1007/s00410-006-0072-9

ORIGINAL PAPER

E. Williams · A. E. Boudreau · S. Boorman
F. J. Kruger

Textures of orthopyroxenites from the Burgersfort bulge of the eastern Bushveld Complex, Republic of South Africa

Received: 9 August 2005 / Accepted: 25 January 2006 / Published online: 16 February 2006

Abstract A suite of 30 samples was collected from the Burgersfort bulge area of the eastern Bushveld Complex for a detailed quantitative textural study. The studied section represents a stratigraphic column approximately 1,000 m thick, of mainly orthopyroxenites from the lower zone (LZ) and lower critical zone. Crystal size distribution (CSD) plots and quantitative fabric analyses reveal a history of crystal aging and compaction, as evident from the loss of smaller-sized crystals and the development of foliation with little evidence of mineral lineation. Compared with the thicker section from Jagdlust (~80 km north), the LZ orthopyroxenites at Burgersfort are consistently finer grained. Foliation is equally well developed at both locations and is consistent with a relatively thin compaction zone at the top of the mush column. Grain size is largely a function of local cooling history with a grain size growth exponent estimated to be between 2.0 and 3.4.

Keywords Bushveld complex · Igneous textures · Igneous compaction

Introduction

It is becoming increasingly recognized that rock textures in layered intrusions can be substantially modified by a variety of post-nucleation mechanisms including crystal aging and compaction (e.g., Hunter 1987; McBirney and Hunter 1995; Waters and Boudreau 1996; Meurer and Boudreau 1998a, b; Higgins 2002b). These works demonstrate that one cannot use observed grain sizes and textures in most plutonic rocks to directly model magma chamber processes without first accounting for these "diagenetic" textural changes.

In an earlier paper of ours, Boorman et al. (2004) documented quantitative textural information through the upper part of the lower zone (LZ) and into the critical zone in the Jagdlust section of the eastern limb of the Bushveld Complex of South Africa. The Jagdlust section hosts the thickest accumulation of these rocks in the entire Bushveld Complex (Cameron 1978). Stratigraphic variations in mineral grain size, rock foliations, modal abundances and residual porosity, as defined by strongly excluded trace elements and abundance of late-crystallizing minerals, were attributed to the combined effects of compaction-induced recrystallization and crystal aging with concurrent crystallization of interstitial liquid.

This study investigates textural variations within a thinner stratigraphic section of the lower and lower critical zones (LCZs) from a different area. Rock textures are compared with those of our earlier study to investigate how rock textures may differ in rocks precipitated from the same magma but subject to a different cooling regime.

Communicated by: T. L. Grove

E. Williams · A. E. Boudreau (✉) · S. Boorman
Division of Earth and Ocean Sciences, Nicholas School of the Environment and Earth Sciences, Duke University, Durham, NC 27708, USA
E-mail: boudreau@duke.edu

S. Boorman
ExxonMobil Upstream Research Company, Fundamental Petrophysics and Geomechanics Section, Old Main Bldg N345, 3120 Buffalo Speedway, Houston, TX 77252, USA

F. J. Kruger
Moruo Mineralogical Services, P.O. Box 432, 1710, Florida, South Africa

Geologic setting

The Bushveld Complex is a layered mafic intrusion in the Republic of South Africa, emplaced ~2,060 Ma (Walraven et al. 1990). It covers an area of about ~66,000 km^2, with the layered portion being ~7–9 km thick. Layering is on all scales, from millimeters to kilometers. A number of stratigraphic zones have been defined (for a summary, see Eales and Cawthorn 1996). Stratigraphically from bottom to top they are: the

Marginal Zone, with norites and pyroxenites showing evidence of crustal assimilation; the LZ, with layers of pyroxenite, dunite, and harzburgite; the economically important critical zone, divided into the LCZ and the upper critical zone (UCZ); and the main and upper zones, consisting primarily of norite and gabbronorite, with some magnetite. The intrusion has several lobes, the main ones being the Western, Potgietersrus, and Eastern.

This study was conducted on a suite of rocks collected from the LZ and LCZ in the eastern lobe of the intrusion. The upper boundary of the LZ is defined as the point at which plagioclase content exceeds ~4%. The LZ here consists primarily of pyroxenites that are part of the Croyden subsuite. The LZ is discontinuous and of variable thickness across the Bushveld Complex (Eales and Cawthorn 1996). In the eastern limb, it reaches a thickness of 1,550 m in the Olifants River tough (Cameron 1978). Our previous study of the LZ–critical zone transition (Boorman et al. 2004) was done on a part of the Jagdlust section from this trough.

Samples for this study were collected from the "Burgersfort bulge", approximately 80 km south of the Jagdlust section. It is so-named because the Bushveld rocks create a map-view bulge in the otherwise semi-circular eastern boundary of the intrusion between the towns of Steelpoort and Burgersfort, where the mafic rocks of the Bushveld Complex are in contact with the sedimentary rocks of the Transvaal supergroup (Fig. 1). This bulge is the result of a shallower dip of 5–10°W in the Burgersfort area as compared with a regional dip of ~15°W elsewhere. The thickness of the LZ is complicated by faulting in the area, but is estimated to be half to two-thirds that of the Jagdlust section

The LZ samples were collected mainly from the flanks of Fraaiuitzicht hill, near the Khumula guest ranch. This hill is east of the Winterveld farm and ~7 km WSW of the town of Burgersfort. Fraaiuitzicht Hill sits in an inverted "V" formed by the intersection of the Steelpoort fault to the west and a fault of unknown type to the east (Walraven 1986). The trace of the Steelpoort fault strikes NE–SW, while the trace of the unnamed fault strikes N–S. The Steelpoort fault is reported to be a brittle, post-emplacement fault (Hatton and von Gruenewaldt 1987). LCZ samples were collected from the Lekyobo hill north of the town of Steelpoort, on the NW side of the Steelpoort fault. Samples collected were considered "typical" for the studied section and unusual textured rocks, such as locally developed pegmatoids, were ignored.

Mineral foliations, where well developed and obvious in the field, were always parallel to regional modal layering, did not have any significant mineral lineations, and did not appear to vary relative to dip direction or the center of the intrusion. This is consistent with paleomagnetic evidence that the Bushveld rocks initially crystallized sub-horizontally and only later acquired their present dip as a result of regional crustal downwarping (Gough and van Niekerk 1959; Eales et al. 1993; Kruger 2005). Because of this, no attempt was

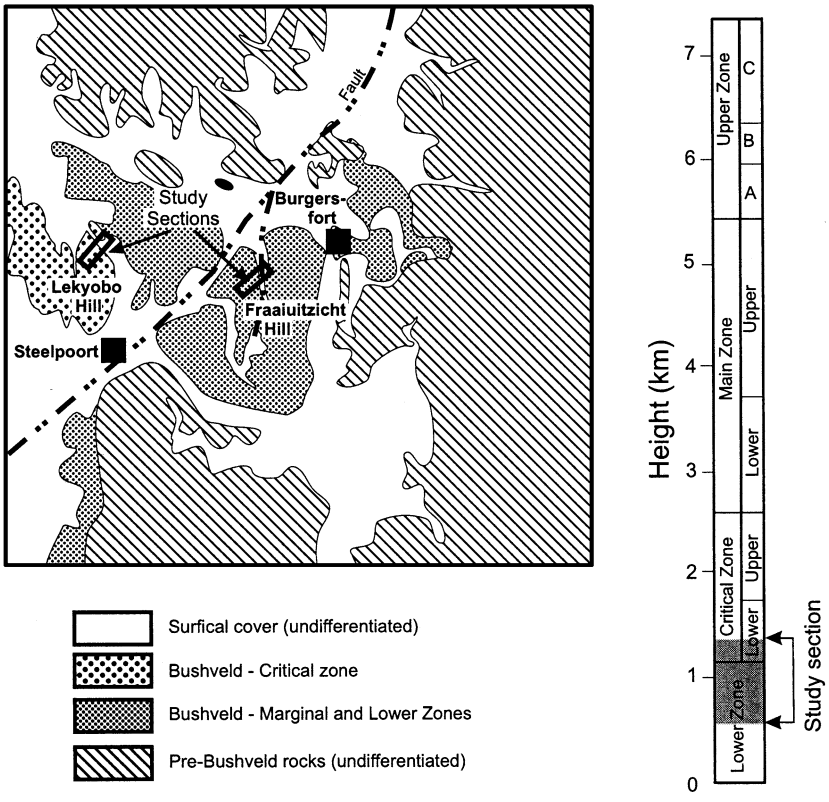

Fig. 1 Geologic map of the "Burgersfort bulge" area of the Bushveld Complex and surrounding rocks, showing locations of the sections used in this study (after Walraven 1986)

made to align sections with respect to dip direction and samples were only marked with an arrow indicating stratigraphic ''up''.

Methods

Texture analysis

Thin sections were prepared to usual standards. Where foliation was visible in hand sample, the sections were cut normal to it (these sections are denoted with an 'N' suffix). Some samples were also cut in a direction parallel to foliation (denoted with a 'P' suffix). Samples with no obvious hand-sample-scale foliation have neither an N nor a P after the number (e.g., sample 89).

Following the method described in Boorman et al. (2004), manual thin section tracings were created as follows. High-resolution digital color photomicrographs are taken of the thin sections in cross-polarized light using a 2,700 dpi film scanner. These scans are enlarged, printed, and placed on a light table. On an overlay, the boundaries of individual orthopyroxene crystals are traced, using a microscope with the original thin section to verify grain boundaries. The smallest grains present (about 0.05 mm) can be clearly seen and outlined at this scale. Areas occupied by another mineral, or by a plucked grain, are left blank. Between 300 and 1,300 grains were traced in each thin section, the average being 690. Samples with larger average grain sizes or lower percentages of orthopyroxene generally have few grains traced.

These tracings are then scanned and imported into Adobe Photoshop, where grain boundaries are digitally cleaned and the grain interiors filled with black. The result is a binary image in which solid black shapes, each representing an individual crystal, are separated by thin white boundaries that represent the original pen lines (Fig. 2).

The Photoshop images for each slide are then analyzed using Scion Image, an image analysis program for the PC. This program measures the area (in pixels) of each separate shape in an image. Each shape is converted into an equivalent ellipse, the area, axes, and orientation (relative to the top of the image) which are recorded.

Using the data produced by Scion, statistics for each sample can be calculated. Percent orthopyroxene is calculated by comparing the total number of black (orthopyroxene) pixels counted by Scion to the total number of white (non-orthopyroxene) pixels in each tracing. A visual estimation is made of the remaining modes. The area of each orthopyroxene crystal is converted into Feret lengths, which is equal to the length of one side of a square with the same area as the crystal. This conversion reduces the effects that irregular crystal shapes have on the calculations. The average grain size for each sample is obtained by averaging the Feret lengths of all the crystals measured. The maximum grain size is defined as the average of the Feret lengths of the largest four grains in each sample. The aspect ratio (AR) is an average of the ARs of the 40 largest ellipses in each sample, calculated by dividing the major axis lengths by the minor axis lengths of those grains.

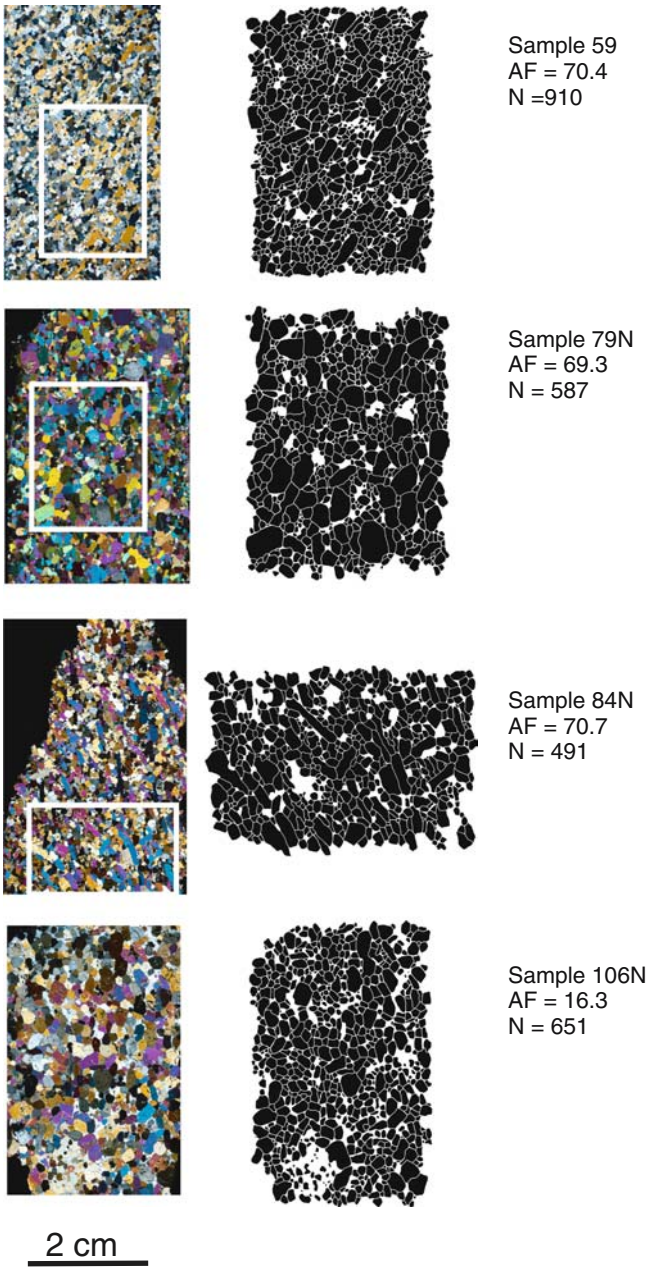

Fig. 2 Samples of binary manual tracings of orthopyroxene grains. Corresponding thin-sections (Cross-polar digital photomicrographs), on left, showing area traced. AF is the calculated alignment factor (AF); *N* as a sample number suffix (e.g., 79*N*) denoted sample cut normal to an obvious foliation; *N* as a variable (e.g., $N = 587$) denotes the total number of grains traced

The alignment factor (AF) enables the strength of the foliation to be quantified. The AF is calculated using the data on 40 largest grains in each sample, since the larger grains primarily define the foliation in these rocks.

To get the AF, the x and y components of the orientation of the major axes of each grain, are put into a matrix, **m**, using the following formula:

$$\mathbf{m} = \frac{1}{N}\begin{pmatrix} \sum x_i x_i & \sum x_i y_i \\ \sum y_i x_i & \sum y_i y_i \end{pmatrix}, \quad (1)$$

where N is the total number of grains measured (Harvey and Laxton1980; Benn and Allard 1989; Meurer and Boudreau 1998a). The eigenvalues of this matrix give the degree of alignment of the grains. These two numbers are normalized to 100. The AF is then calculated as

$$\mathrm{AF} = (e_1 - 50) \times 2, \quad (2)$$

where e_1 is the larger of the two eigenvalues (Meurer and Boudreau 1998a). An AF of 100 indicates a perfect alignment of crystals and a value of 0 indicates a random arrangement with no alignment.

Crystal size distribution (CSD) plots were created using Michael Higgins's CSD Corrections program, version 1.35 (Higgins 2000). CSD Corrections takes crystal sizes in 2D and calculates theoretical 3D crystal sizes, taking into account the fact that the data were collected from a cut section. However, because the program does not constrain calculated values to the observed mode and can give significant errors for non-equant crystals (Boorman et al. 2004), grains were entered as cubes with sides equal to the Feret lengths as calculated from the Scion data. Plotting corrected crystal size versus the natural log of the population density yields the CSD plot. Imposing a best-fit line over the main trend of these plots (using the "plot line" function in CSD Corrections, but hand-removing the points that visibly fall off the linear trend at the smaller sizes) gives a slope and an intercept for each graph. CSD Corrections also generates a peak size reading, which is the size bin with the largest number of crystals in it.

Geochemistry

Major element abundances were determined by direct current plasma optical emission spectrometry (DCP-OES). Samples were prepared by the methods of Klein et al. (1991) on an ARL Fisons spectroscan 7 DCP at Duke University. Trace element abundances were obtained by inductively couple plasma mass spectrometry (ICP-MS) using a VG-Elemental Quadropoe-3 system at Duke University. Sample digestion and operating parameters have been described by Meurer and Boudreau (1998b).

A total of 31 samples were analyzed using this process. They include most of the samples that were analyzed for texture, but also include some that were not. Based on the major element analysis, whole-rock Mg# (= Mg/(Mg + Fe), molar) was calculated for samples and plotted against relative stratigraphic position. CIPW norms were calculated from the whole-rock major element data using PELE (Boudreau 1999). Feldspar content, based on the total of anorthite, albite, and orthoclase from the norm, was plotted against relative stratigraphic height.

Samples

The samples of the Burgersfort column are divided on the basis of mineralogy and texture into three main groups (Fig. 3). Group 1 is by far the largest, with 19 of the 26 samples falling into this category. Samples from Groups 1 and 3 were analyzed for texture.

Group 1

Group 1, which comprises most of the samples (59, 60, 64, 66, 67, 68, 69, 71, 72, 74, 76, 77, 78, 79, 80, 84, 88, 89, 100, 101, 103), typically contain >85% orthopyroxene,

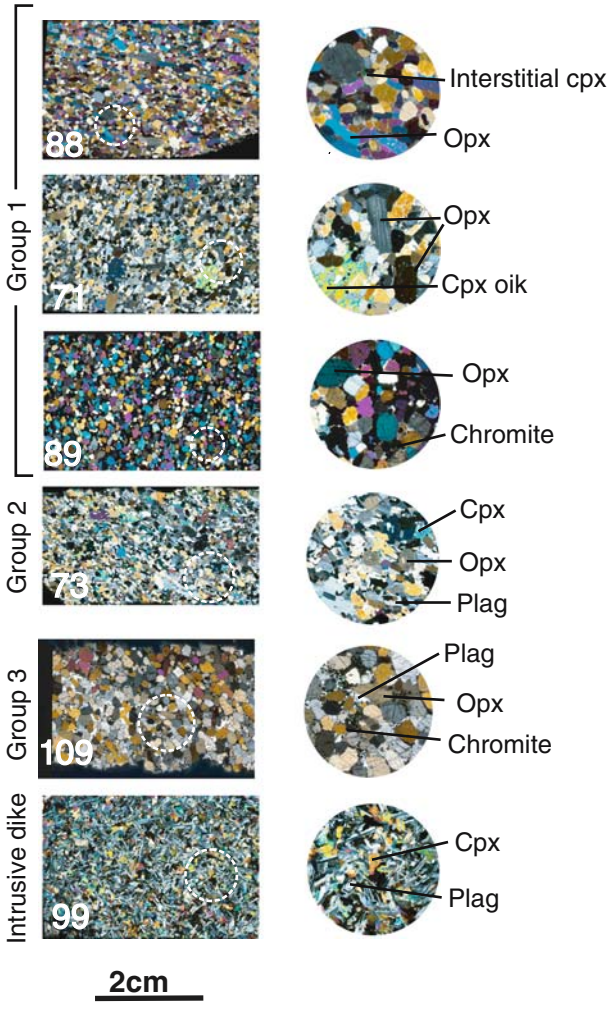

Fig. 3 Textural groups of the Burgersfort samples. *Dashed white circles* in the left column indicate the area of close-up view on the right. Also shown is a late cross-cutting mafic dike for comparison. *Scale bar* refers to all images in the left column; note that scales in the right column vary. Cross-polar digital photomicrographs

with or without small amounts of clinopyroxene, euhedral olivine, plagioclase, or chromite. Although mainly typical of LZ orthopyroxenites, the Group 1 samples are found throughout the column, and are equivalent to the Group 1 samples of Boorman et al. (2004). The orthopyroxenes are tightly packed sub- to euhedral grains, with orthopyroxenes in contact with other orthopyroxenes along most grain boundaries. Grain sizes range from about 0.2 mm to several millimeters in length, with an average of about 0.5 mm. There are patches of interstitial clinopyroxene, making up less than 5% of the area. Samples 64, 68, 69, 71, 72, 74, 78, 84, 101, 103 also have $<5\%$ interstitial plagioclase. These samples are interspersed among the ones with only trace plagioclase, with no apparent pattern. One sample (84) collected near the Lower Group 6 chromitite (LG-6), has a small amount ($<5\%$) of chromite as well. Small equant chromite grains occur between the orthopyroxenes throughout the sample. In some samples, particularly samples 69, 71, and 77, clinopyroxene oikocrysts several millimeters in diameter enclose noticeably smaller crystals of orthopyroxene.

Sample 89, ~40 mode % chromite, is also placed in this group. It is texturally similar to others ion this group except for the higher percentage of chromite. Small chromite grains cluster between relatively equant orthopyroxenes. This sample shows no obvious foliation.

Group 2

Group 2 is represented only by sample, 73, and contains ~40% euhedral plagioclase, ~20% orthopyroxene and and 20% clinopyroxene, making it a gabbronorite. In thin section, chains of touching orthopyroxene crystals are separated by subhedral plagioclase. Subhedral clinopyroxenes are similar in size to the orthopyroxenes. Many of the orthopyroxenes and clinopyroxenes are embayed by feldspar. This sample was not analyzed for texture and is included only for comparison with Boorman et al. (2004).

Group 3

The two samples of Group 3 (106 and 109) are orthopyroxenites with a higher percentage of interstitial plagioclase (~10–15%) than seen in the Group 1 samples. These modes are typical of LCZ rocks, where plagioclase is a more obvious interstitial phase. They are equivalent to the Group 3 samples of Boorman et al. (2004). Sample 109 has about 10% chromite surrounding the orthopyroxene grains, while 106 has no chromite. Some orthopyroxene grains are embayed by plagioclase. These orthopyroxenes crystals are both larger (>0.8 mm average size) and more equant than in the Group 1 samples. In addition, the grains are of a more consistent size, with fewer small crystals than in other samples.

Grains of all groups show evidence of post-crystallization processes that have modified the textures; some of the more obvious are illustrated in Fig. 4. These include optically continuous grains that appear to have been separated into two or more smaller grains (Fig. 4a, d) and the development of sub-grains within larger grains (Fig. 4b, c). For textural analysis, clearly separated grains are counted as separate grains, whereas subgrains developed in larger grains are incorporated into the larger grains as shown by the heavier dashed outlines in Fig. 4.

Some samples have an annealed texture in which orthopyroxene grains meet at near-120° boundaries, with no interstitial material. Other samples have a range in grain sizes, in which the larger grains are surrounded by much smaller ones. Foliation, defined by the shape-preferred orientation of the larger orthopyroxene grains, is qualitatively variable from weakly to strong. Finally, both the extent of foliation and the local average size of the grains can vary even on the scale of a single thin section. Except as noted, we report the average for the total thin section area studied.

Results

Texture

The results of the textural analysis are summarized in Fig. 5 and Table 1. Crystal size is measured in three different ways: by peak size bin, average size (L_{avg}), and maximum grain size (L_{max}). The L_{max} graph (average of four largest grains) shows no consistent trend and values scatter between 1.5 and 2.1 mm. The L_{avg} plot, however, shows an increase in average crystal size with up-section from 0.40 to 0.55 mm, with the two samples from the LCZ (106 and 109) being significantly larger (>0.8 mm) than the stratigraphically lower samples. The peak size bin measurements from CSD Corrections show a similar trend as L_{avg} and similar, though slightly higher, ranges.

The CSD plots for all samples all have negative slopes and turn down at the lower size bins (Fig. 6). CSD shapes and ranges are fairly consistent but with local deviations from the main trend. The notable exceptions to the overall similarity are the only two samples in Group 3 from the lower part of the LCZ. They have significantly shallower slopes and lower intercepts than the others, which are consistent with the larger grain size size of these samples noted above. CSD slopes and intercepts plot as a linear array, indicating CSD closure (Fig. 6, inset) (Higgins 2002a). Excluding the two uppermost LCZ samples (Group 3) and the chromitiferous Group 1 sample (89), the ortho-pyroxenite CSD slopes range from -5.9 to -4.0, with an average of -5.1, and intercepts range from 3.5 to 4.9. Overall, CSD slopes become flatter and intercept values decrease up-section to produce counter-clockwise rotation of the log-linear portions of the CSDs as a function of stratigraphic

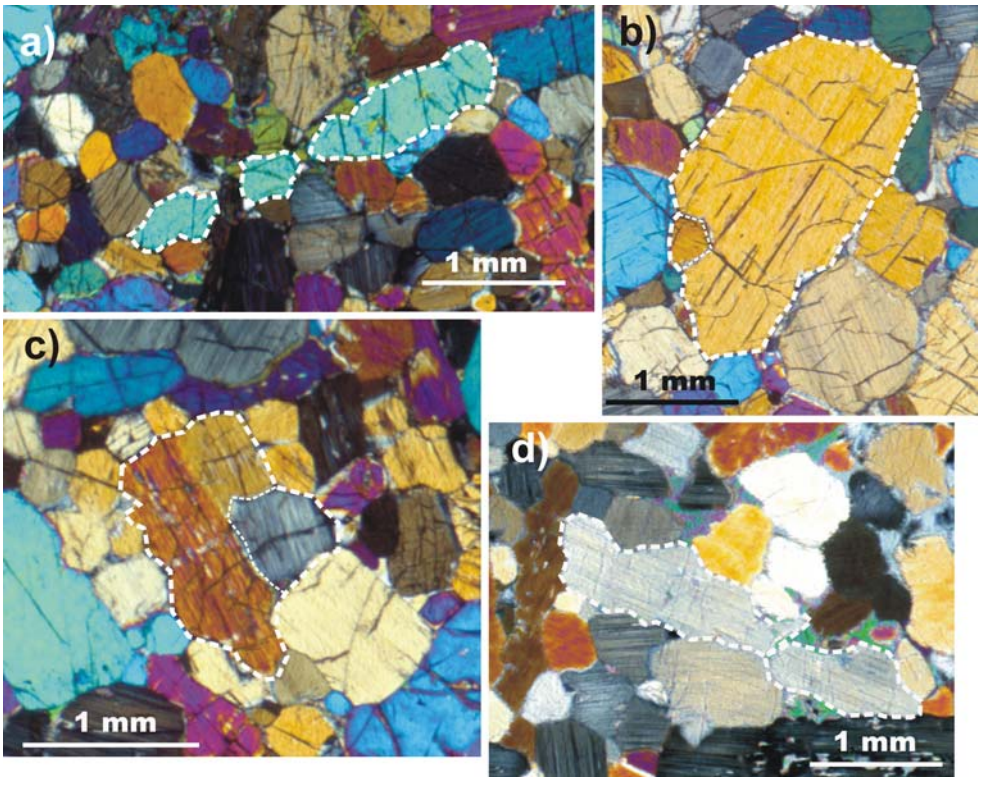

Fig. 4 Orthopyroxene grains with evidence of textural modification, illustrating some of the problems for quantitative textural analysis. **a** Optically continuous grain that appears to have separated into three smaller grains. **b** and **c** Sub-grains within larger grains. **d** Long optically continuous grain, broken into two smaller grains. For textural analyses, no attempt was made to reconstruct possible broken grains but sub-grains (*light dashed outlines*) were included as part of a single, larger grain (*heavy dashed outlines*). Cross-polar digital photomicrographs

height. Again, this is consistent with an increase in grain size with stratigraphic height.

AF data show moderately well developed foliation of the larger crystals in most samples. AFs for sections cut normal to foliation range between 20 and 80, and average 54. The chromite-rich sample 89 is an exception, with an AF of 13.7. The samples in the lower two-thirds of the section generally show an increase in AF up-section. A few samples were analyzed for mineral alignment both normal and parallel to foliation. AF parallel values are invariably low even is those samples with high AF normal values, indicating a lack of lineation (Fig. 7).

AR range from 1.58 to 3.12, with an average of 2.39. There is no discernible trend to the data, although, like the AF graph, the stratigraphically highest six samples show significantly lower ARs than the others. The AR of the chromite-rich sample (89) is the lowest of the group.

Othropyroxene crystals hosted by four clinopyroxene oikocrysts from one sample (71oik, Table 1 and Fig. 6) were also examined. A total of 65 orthopyroxene chadacrysts were measured (in the same way that the whole-slide data was collected for the other samples) in order to compare their textures to the textures of the crystals in the remainder of the rock. The L_{avg} of the chadacrysts is 0.211 mm, about half the value for the lowest L_{avg} reported in Table 1. L_{max} is 0.553 mm, about one-third that of the lowest L_{max} for the whole slides. The AR, 2.04, is similar to the average for the rest of the samples. An AF of 14.6 for the chadacrysts is quite low. Even comparing these data to the slide from which they are taken (71*N*), the differences are clear. Outside of the oikocrysts, sample 71*N* has an L_{max} of 1.5 mm; AR is 2.74; AF is 50.1; peak size is 0.562 mm; L_{avg} is 0.4 mm. CSD data may not be significant based on so few points; however, the plot lacks the turn-down at smaller crystal lengths seen in all the other CSDs and has a higher intercept (5.37) and steeper slope (−9.07). Although only one sample with oikocrysts was measured in this way, the results are consistent with visual impressions that the orthopyroxene in the oikocrysts has pobvious different textural characteristics than the host.

Comparison with Jagdlust

The Burgersfort samples show both similarities and differences when compared with the stratigraphic section at Jagdlust studied by Boorman et al. (2004) (Fig. 9). For example, in both sections the grain sizes are remarkably uniform in the portions of the LZ studied. However, in all three measures of crystal size, the

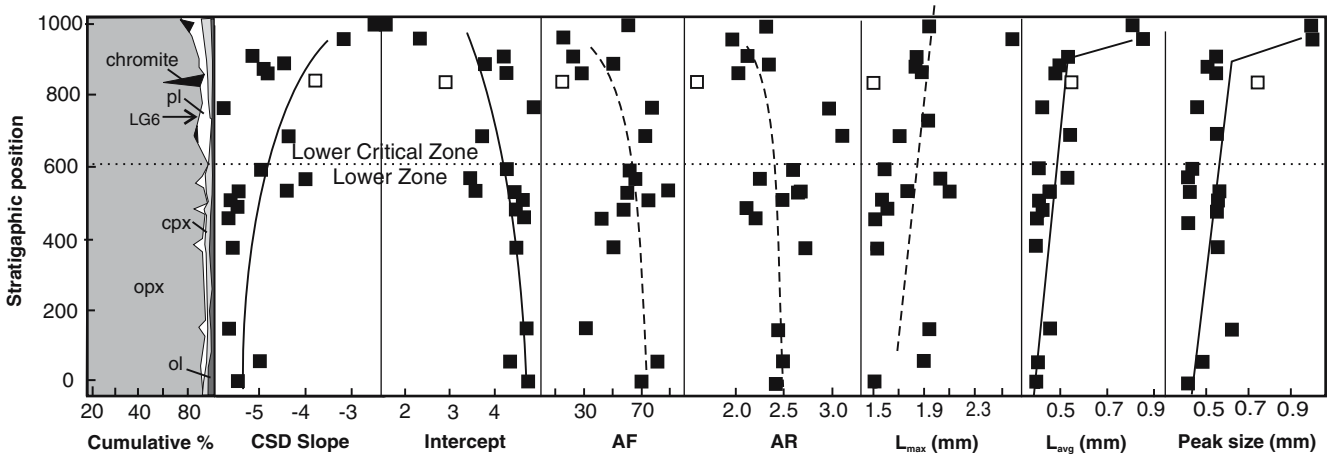

Fig. 5 Summary of textural data. From the left, plots are of mineral modes, orthopyroxene CSD slope and CSD intercept, orthopyroxene AF, orthopyroxene aspect ratio (AR), maximum of three largest orthopyroxene grains (L_{max}), average orthopyroxene grain size (L_{avg}), and orthopyroxene grain size of the peak CSD bin (peak size). *Open square* is a chromite-rich sample

Burgersfort section LZ orthopyroxene grains are smaller than the Jagdlust grains. Thin-section-scale observation confirms this result. L_{max} is 2–3 mm for Jagdlust and 1.5–2.1 mm for Burgersfort. L_{avg} is around 0.75 mm for Jagdlust and around 0.5 mm for the Burgersfort samples, which show a slight increase up-section. Peak size for Jagdlust LZ orthopyroxene is ~0.7 mm and Burgersfort numbers are ~0.5 mm. Furthermore, orthopyroxene grain size is typically larger in the LZ than in the LCZ in the Jagdlust section, whereas there is generally an increase in grain size with height in the Burgersfort area. This results in the rock textures for LCZ samples being roughly similar in both areas.

The CSD plots of this study are qualitatively similar with those of Boorman et al. (2004), with both sections characterized by a straight line at higher crystal sizes, and a concave-downward bending at smaller crystal sizes. However, the CSD slopes of the Jagdlust LZ cluster from −2 to −4 and are significantly higher than seen the Burgersfort samples (−3 to −6, Fig. 9).

Table 1 Tabulation of textural data from the Brugersfort bulge area of the Bushveld Complex

ID	Height (m)	Zone	CSD		L_{avg}	Aspect ratio	Peak size	L_{max}	N	Mode % opx	Alignment factor
			Slope	Intercept							
109	1,000	LCZ	−2.45	1.62	0.81	2.32	1.00	1.95	372	72.1	61.0
106*N*	960	LCZ	−3.04	2.34	0.85	1.97	1.00	2.71	651	81.5	16.3
103	900	LCZ	−4.44	3.77	0.54	2.11	0.56	1.86	558	88.7	24.1
101	880	LCZ	−4.90	4.29	0.50	2.34	0.52	1.85	633	87.8	51.1
100	870	LCZ	−4.85	4.29	0.49	2.03	0.56	1.90	595	93.5	28.9
89	840	LCZ	−3.80	2.94	0.55	1.58	0.75	1.47	445	58.9	13.7
88*N*	780	LCZ	−5.86	4.86	0.44	2.96	0.46	1.95	822	90.1	77.0
84*N*	700	LCZ	−4.35	3.75	0.55	3.12	0.56	1.71	491	85.2	70.7
80*N*	600	LZ	−4.99	4.28	0.42	2.58	0.42	1.56	822	94.4	59.3
79*N*	580	LZ	−4.00	3.47	0.53	2.23	0.42	2.07	587	89.4	65.3
78*N*	550	LZ	−4.43	3.63	0.45	2.67	0.56	1.76	567	85.4	88.2
77*N*	540	LZ	−5.43	4.47	0.45	2.64	0.42	2.15	652	90.8	59.4
76*N*	510	LZ	−5.64	4.7	0.40	2.47	0.56	1.56	849	96.2	56.8
74*N*	480	LZ	−5.48	4.49	0.43	2.10	0.56	1.59	803	82.9	74.9
72*N*	450	LZ	−5.71	4.72	0.40	2.21	0.42	1.48	878	93.7	42.3
71*N*	390	LZ	−5.60	4.56	0.40	2.74	0.56	1.50	922	82.8	50.1
71oik	390	LZ	−9.07	5.37	0.21	2.04	0.51	0.55	65	(82.8)	14.6
64	150	LZ	−5.68	4.76	0.45	2.44	0.63	1.97	662	89.5	31.3
60*N*	60	LZ	−4.99	4.37	0.42	2.46	0.49	1.90	631	89.8	79.6
59	0	LZ	−5.52	4.77	0.40	2.43	0.42	1.50	910	91.1	70.4
	Averages		−4.80	4.00	0.50	2.39	0.57	1.81	676	86.5	53.7

"*N*" after sample ID number denotes sample cut normal to foliation; "oik" after sample ID number indicates only grains entrained in clinopyroxene oikocrysts were measured. Heights are relative to the lowest sample of the section. Slope and intercept vales for the CSD plots are for the log-linear portions of the CSD curve

LZ lower zone, *LCZ* lower critical zone, L_{avg} average Feret size, L_{max} average of four largest grains, *peak size* CSD bin with largest grains, *aspect ratio* ratio of major to minor axis of best fit ellipse (see the text), *N* total number of grains measured, *alignment factor* AF for 40 largest grains of a given sample

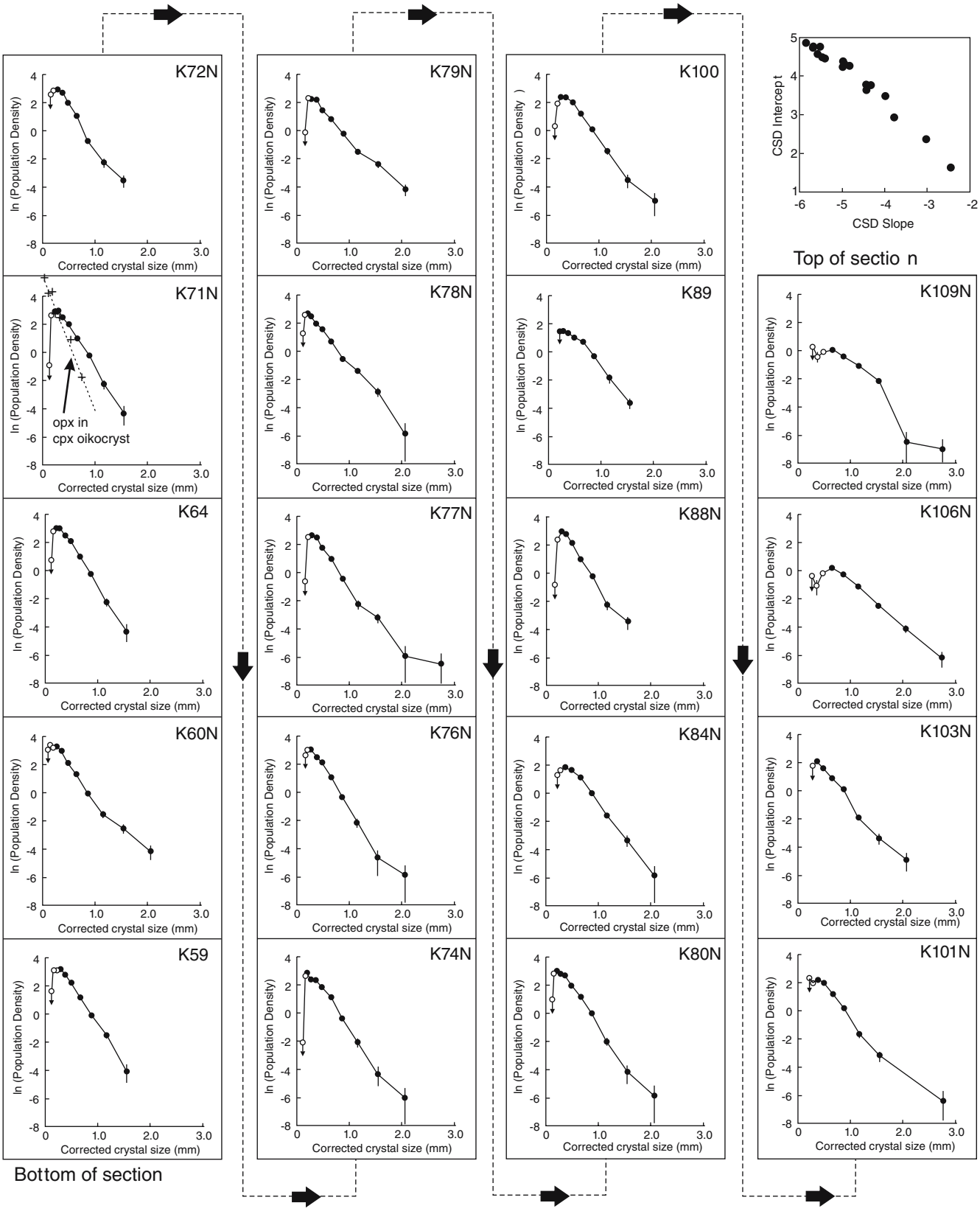

Fig. 6 CSD plots for 19 samples. Lowest sample in column is at bottom left, highest is at top right. Same scale for each graph. Inset at upper right shows plot of intercept versus slope for the log-linear best fit line for each graph: best fit lines for slope and intercept values are fit to the *solid symbols* only and are listed in Table 1 and also shown in Fig. 5. The '+' symbols and the *dashed line* added to sample 71*N* are data for orthopyroxene enclosed in a clinopyroxene oikocrysts (sample 71oik of Table 1). Note overall flatter slopes with an increase in stratigraphic height. See the text for additional discussion

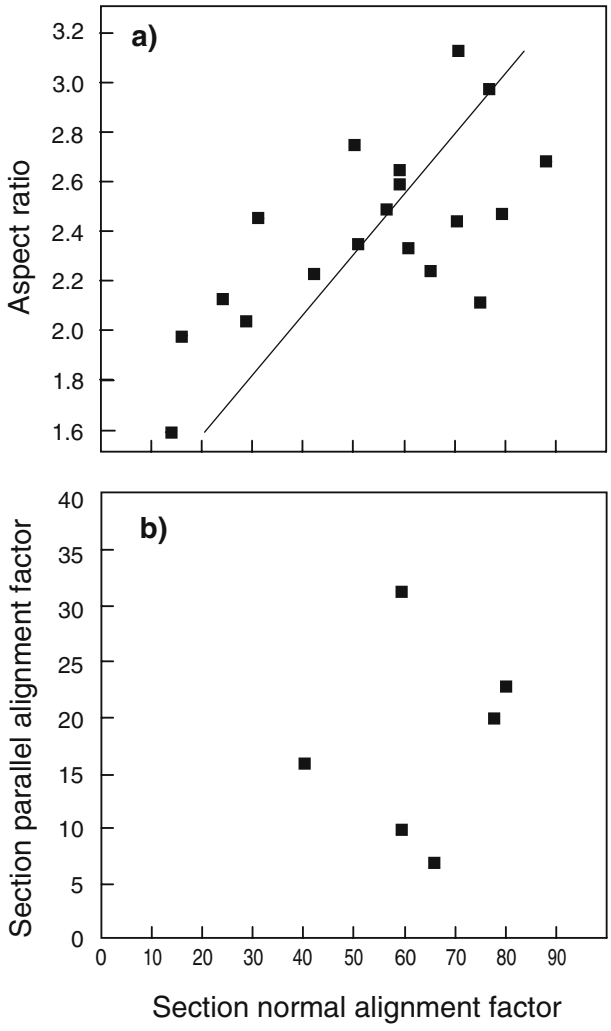

Fig. 7 Plots of **a** AR of orthopyroxene and **b** AF of orthopyroxene parallel to layering, both plotted against the AF of orthopyroxene on sections cut normal to layering. Note the lack of significant alignment in the plane of layering even in well-foliated rocks with minerals with high ARs, demonstrating a lack of lineation

The Jagdlust data show no significant trend in the LZ, while the Burgersfort data show a slight decrease in CSD slopes. The CSD intercepts are somewhat higher for the Burgersfort data than for the LZ at Jagdlust (3–5 and 2–4, respectively, not shown in Fig. 9). Again, the Burgersfort data show a trend that is opposite to the trend of the Jagdlust data, although the Jagdlust trend is weak. Overall, however, the Burgersfort CSD LZ trends represent smaller grain size as compared with the Jagdlust rocks.

The AF data for the LZ in both areas tend to be similar, clustering around 70 with a few lower values, particularly in the Burgersfort area. The ARs for the LZ at Jagdlust are all around 2.0, while the Burgersfort ARs are higher, at 2.5(Fig. 9). Both sections show a broadly positive correlation between foliation and AR, even the LCZ samples (Fig. 7a and Fig. 7a of Boorman et al. 2004). In contrast, the degree of foliation is only weakly correlated with grain size between the two regions; while foliation is variable in both regions, it can be as well-developed in the fine-grained Burgersfort rocks as in coarser-grained Jagdlust rocks.

Geochemistry

Geochemical data are tabulated in Table 2 and plotted in Fig. 8, where Mg# and normative plagioclase content are compared with those from the Jagdlust section. The Burgersfort orthopyroxenites have Mg#s between 0.80 and 0.86. A small repeated increase up-section is seen between 50 and 450 m, and again from 450 to the top of the LZ. Percent normative feldspar, here used as a proxy for the amount of crystallization of late (post-orthopyroxene) minerals, ranges between 3.6 and 36; the outlier is the group 2 sample. Overall, however, the geochemical profile is unremarkable.

The LZ Burgersfort Mg#'s are slightly lower and show more variation than the Jagdlust samples, the latter ranging narrowly between 0.85 and 0.86. However, the Lower of the Jagdlust section has only six samples, representing ~200 m, so the full range was not sampled there. The slight decrease in Mg# reported for the Jagdlust LCZ samples is similar in magnitude to the slight decrease seen in the upper three samples from Burgersfort. There is less variability in the upper three samples (100, 101, 103), but no large difference between them and the previous samples in this part of the section, as might be expected since their Mg# numbers differ noticeably from those of the rest of the LZ samples. Normative feldspar content is similar to slightly higher than that reported for the Jagdlust column.

Discussion

As observed in the Jagdlust section, the rocks of the Burgersfort region are variably foliated but are not significantly lineated. In the Jagdlust study, it was suggested that the textural features were the result of compaction-driven recrystallization and crystal aging in a cooling and crystallizing crystal + liquid assemblage (Boorman et al. 2004). It is suggested that much the same processes acted in the Burgersfort area as well. During compaction, a mineral alignment can develop and in other studies the AF has been used to investigate compaction efficiency (e.g., Meurer and Boudreau 1998a). AR will also increase during compaction due to preferential growth of crystals aligned to accommodate the local stress field (Maaloe 1976; Mathison 1987). The correlation of AF and AR for the Burgersfort samples indicate that compaction along with crystal aging has led to larger crystals and increased foliation (Meurer and Boudreau 1998a).

The lack of lineation in the Burgersfort column indicates that neither stretching nor flow associated with

Table 2 Major element analyses from the Brugersfort Bulge area of the Bushveld Complex

Sample	Height	Zone	SiO_2	TiO_2	Al_2O3	Fe_2O_3	MnO	MgO	CaO	Na_2O	K_2O	P_2O_5	Sum	Cr	Mg#	An + Ab + Or
59	0	LZ	54.97	0.12	1.42	10.96	0.22	30.03	2.03	0.05	0.01	0.03	100.00	4,288	0.844	4.13
60	60	LZ	54.45	0.11	1.26	12.12	0.24	29.25	1.93	0.02	0.00	0.03	99.47	3,302	0.827	3.6
61	90	LZ	54.99	0.11	2.07	11.68	0.23	28.89	2.19	0.09	0.00	0.03	100.45	3,155	0.830	6.05
62	110	LZ	54.59	0.13	2.98	12.09	0.23	27.03	2.63	0.25	0.03	0.03	99.75	3,010	0.816	9.32
63	130	LZ	54.68	0.12	2.59	10.67	0.21	28.31	2.45	0.17	0.08	0.02	99.48	3,658	0.840	8.13
64	150	LZ	54.61	0.10	2.64	10.14	0.20	28.19	2.64	0.17	0.03	0.02	99.20	4,451	0.847	8.15
65	190	LZ	54.00	0.11	2.85	9.96	0.20	28.70	2.59	0.18	0.07	0.02	99.13	4,043	0.851	8.91
66	230	LZ	54.43	0.10	1.48	10.51	0.20	29.22	1.93	0.08	0.02	0.02	98.42	4,663	0.846	4.54
67	270	LZ	54.58	0.10	1.41	10.15	0.20	30.33	2.01	0.03	0.02	0.03	99.42	5,276	0.856	4.14
68	320	LZ	54.84	0.10	1.61	10.18	0.20	29.76	2.01	0.09	0.02	0.03	99.41	5,175	0.853	4.9
69	360	LZ	54.72	0.11	2.17	9.31	0.19	28.82	3.59	0.19	0.03	0.03	99.52	4,188	0.860	6.87
71	390	LZ	54.49	0.09	4.64	8.99	0.19	26.78	4.96	0.25	0.03	0.03	100.23	4,464	0.855	13.83
72	450	LZ	55.71	0.10	2.00	9.66	0.20	29.72	2.52	0.14	0.02	0.03	100.08	3,988	0.859	6.1
73	470	LZ	52.53	0.09	11.52	8.43	0.18	17.36	9.82	0.80	0.06	0.03	100.86	1,273	0.803	34.8
74	480	LZ	53.41	0.08	4.12	10.84	0.22	26.92	3.25	0.18	0.01	0.03	99.51	3,728	0.831	12.24
76	510	LZ	54.30	0.09	1.70	11.51	0.23	29.53	1.73	0.04	0.01	0.03	99.54	4,777	0.836	4.91
77	540	LZ	54.13	0.09	1.57	10.97	0.22	29.89	1.83	0.02	0.01	0.03	99.24	4,531	0.844	4.52
78	560	LZ	53.77	0.08	6.70	8.86	0.17	25.44	4.11	0.33	0.03	0.03	99.97	3,009	0.850	19.94
79	580	LZ	53.99	0.09	1.57	10.72	0.20	29.27	1.63	0.06	0.02	0.03	98.11	3,793	0.844	4.74
80	600	LZ	54.75	0.09	1.56	10.52	0.21	30.22	1.59	0.03	0.01	0.03	99.50	4,763	0.851	4.51
82	650	LCZ	55.08	0.10	1.90	9.82	0.20	30.09	2.24	0.09	0.00	0.04	99.98	4,794	0.859	5.61
84	700	LCZ	54.45	0.14	2.25	10.90	0.21	28.86	2.28	0.14	0.00	0.03	100.45	10,617	0.842	6.85
89	840	LCZ	36.29	0.25	6.00	14.13	0.19	21.53	1.53	0.10	0.01	0.04	85.16	51,503	0.751	10.45
100	870	LCZ	54.63	0.11	1.82	12.34	0.24	28.78	2.05	0.07	0.01	0.03	100.69	6,928	0.822	5.35
101	880	LCZ	54.85	0.11	1.84	12.33	0.24	28.60	1.98	0.12	0.02	0.03	100.70	5,705	0.821	5.64
103	900	LCZ	54.38	0.11	1.69	12.32	0.24	28.61	2.05	0.07	0.03	0.03	99.93	6,629	0.821	5.08

simple shear has occurred; therefore, a pure shear as expected in one-dimensional compaction is the preferred interpretation. This is consistent with paleomagnetic evidence that the Bushveld rocks initially crystallized sub-horizontally and did not experience any down-slope flow which could impart a lineation.

The Burgersfort CSDs are also consistent with a crystal aging of the mineral assemblage. With constant growth and nucleation rates, CSD of primary magmatic textures should be log-linear (Marsh 1998). The lack of the smaller grains sizes to produce a turned-down CSD is consistent with the loss of a population of crystals with smaller sizes as crystals combine after initial crystallization (Higgins 2002a; Boorman et al. 2004).

Oikocrysts growth around previously crystallized grains can preserve earlier crystallization textures by surrounding and isolating of these grains and limiting recrystallization (e.g., Mathison 1987; Higgins 1998). Therefore, chadacrysts can be a better measure of original crystallization textures than the surrounding rock, which may have undergone substantial post-crystallization modification. The orthopyroxene chadacrysts of sample 71*N* certainly point to this interpretation, as their textures are markedly different from the textures of the grains outside of the oikocrysts. Compared to the surrounding rocks, the chadacrysts are smaller, more equant, and unaligned. Their significantly lower alignment (AF) and sizes are interpreted to be closer to the original textures than those of the remainder of the rock. The lack of a turn-down in the smallest chadacryst lengths in the CSD plot is consistent with those smaller sizes having been present in the original texture and were not simply the result of melt being expelled from the system before it could crystallize a large number of small crystals (Marsh 1998). The steep slope of the chadacryst CSD as compared with the surrounding grains is also typical of the counter-clockwise rotation expected from crystal aging.

The observation that both the Burgersfort and Jagdlust sections have developed similar degrees of foliation development independent of grain size suggests that compaction reduced initial porosity rather quickly. This is consistent with a number of studies (e.g., Shirley 1986) that much of the compaction in a growing mush column occurs relatively quickly in a relatively thin zone at the tip of the mush column where residual liquid can be easily expelled out the top of the crystal pile. Further, the similar amount of interstitial plagioclase in orthopyroxenites from the two sections implies that compaction was equally effective at reducing porosity to roughly the same degree in both areas.

Although initial porosity of the orthopyroxenites appears to have been quickly reduced (but not eliminated prior to the crystallization of later phases such as plagioclase) in both the Burgersfort and Jagdlust sections, the rock continued to experience an extended period of high temperature annealing. The grain size difference is attributed to the thinner Burgersfort section as compared with that at Jagdlust, which allowed more time for aging processes to enlarge grain size. More extensive aging apparently resulted in a lower crystal AR in the Jagdlust section as well. It should also be noted

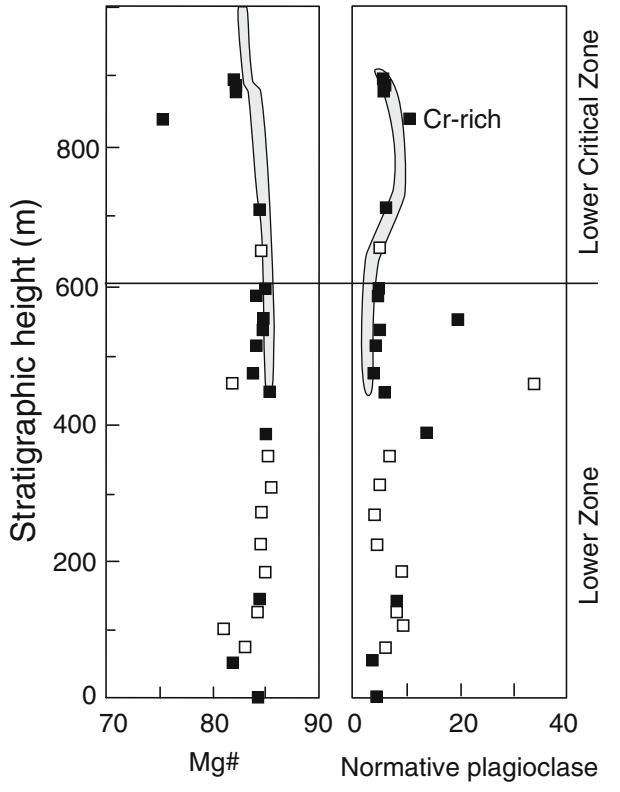

Fig. 8 Mg#, [molar Mg/(Mg + Fe) ratio] and normative feldspar abundance of Lower Zone (LZ) samples, plotted against stratigraphic height. The normative feldspar content is based on CIPW Norm calculations and is equal to AB + AN + OR. *Filled squares* are those for which textural data was collected and presented in the previous figures, *open squares* are samples for which there is compositional data alone. *Shaded fields* show ranges from orthopyroxene-rich samples from the Jagdlust section (Boorman et al. 2004)

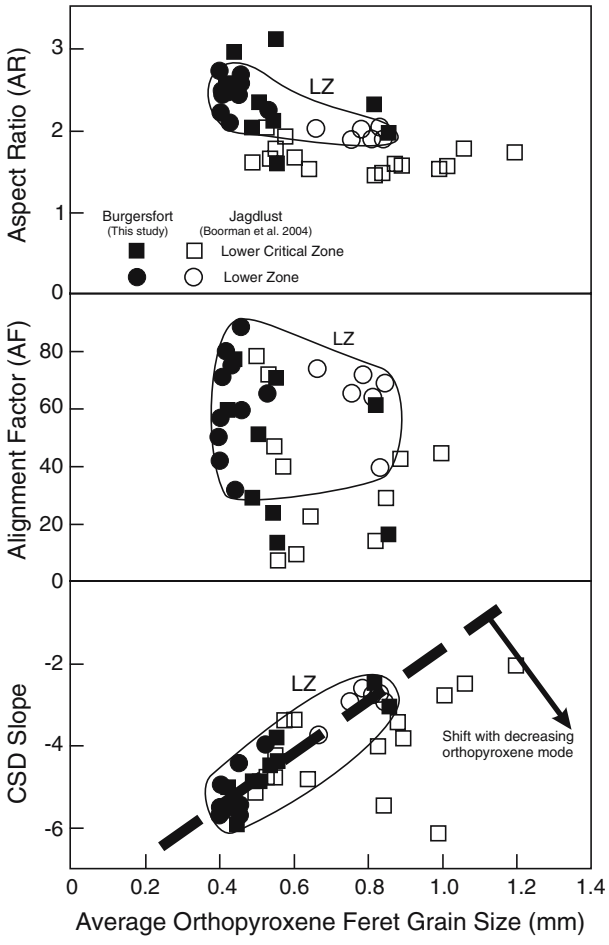

Fig. 9 Comparison of orthopyroxene textural data from Burgersfort areas (*solid symbols*, this study) with that from the Jagdlust areas (*open symbols*; data from Boorman et al. 2004). *Circles* are LZ samples, *squares* are lower critical zone samples. *Solid outline labeled 'LZ'* is the field for LZ samples from both regions. *The heavy dashed line* in the CSD slope plot is visual fit to LZ samples, which have the highest average mode percent orthopyroxene. This line would shift in the direction of *arrow* with decreasing mode percent orthopyroxene. See the text for additional discussion

that the development of coarser rocks in the thicker section implies that processes that lead to mineral growth (e.g., crystal aging and compaction-induced recrystallization) dominate processes that tend to reduce grain size in a compacting crystal pile as illustrated in Fig. 4.

Orthopyroxenites from the LZ near the LZ–LCZ contact of the Jagdlust area are about 50% larger than those from the equivalent stratigraphic region in the Burgersfort area (average Feret sizes = ~0.5 and ~0.75 mm, respectively; Fig. 9). What does this size difference say about the time scale of crystal aging between the two sections?

In a recent paper, Faul and Scott (2006) summarize the controls on the time scales of crystal aging. In general, the time scale is an exponential function of grain size:

$$L_t^n - L_0^n = Kt, \tag{3}$$

where L_0 is the grain size at time $t = 0$, L_t is the grain size at time t and K is a rate constant. The growth exponent, n, typically varies between 2 and 4 and is a function of the different types of kinetic controls on mineral grain growth. These growth laws are for growth by aging only and do not include other forms of stress-inducted recrystallization as can occur in a compacting crystal pile.

If it is assumed that all post-accumulation grain recrystallization in the Bushveld is limited by the cooling rate of the crystal pile, and that the cooling is primarily by thermal diffusion, then the time for recrystallization by aging and compaction will scale to the square of the distance. Thus, for the Jagdlust section, which is approximately 50–100% thicker than that of the Burgersfort, the thermal time scale will increase by a factor of 2.2–4.0. If it is assumed that L_0 of Eq. 3 is zero for both the Jagdlust and Burgersfort sections, then one can equate average grain size between the two sections by the following relation:

$$\left(\frac{L_t^{\text{Jagdulst}}}{L_t^{\text{Burgersfort}}}\right)^{n} = \frac{t^{\text{Jagdlust}}}{t^{\text{Burgersfort}}} = 2.2 - 4.0. \quad (4)$$

Using the observed average orthopyroxene grain size ratio between the two regions of 1.5, then the growth exponent, n, in Eqs. 3 and 4 should be between 2.0 and 3.4. (If L_0 is not zero but otherwise the same for both sections, then the ratio on the left hand side of Eq. 4 will increase and the growth exponent will be lower. If L_0 is nonzero but scales with L_t between the two regions—i.e., the quicker-cooled Burgersfort region nucleated more but smaller grains—then the value of n will be approximately the same.) These estimated values fall within the range of theoretical and experimental values for the growth exponent noted above, and compare with experimentally determined growth exponent ranging from 2 to 4.3 measured in aging olivine aggregates (Karato 1989; Nichols and Mackwell 1991; Faul and Scott 2006). As noted by Faul and Scott (2006), growth rates can be influenced by a number of factors, including the amount of melt present, the presence of other solid phases, and especially the presence of volatile fluids. Regarding the latter, the presence of pegmatoidal layers throughout the Bushveld suggests that some of the size variations in the individual sections might have been caused by local variations in volatile content. In any event, the calculated aging growth rates appear reasonable.

Conclusions

The Burgersfort textures, as represented by the CSDs, AFs, and ARs, all indicate significant post-crystallization, compaction-driven recrystallization and crystal aging. This post-crystallization alteration is compatible with uniaxial compaction with no significant component of shear and is consistent with an original sub-horizontal crystallization of the Bushveld rocks. It is suggested that where mineral lineation accompanies a well-developed foliation (e.g., Higgins 2002b), such textures may reflect compaction with a slip component related to crystallization on a sloping solidification front and need not be prima facie evidence of deposition from a flowing magma.

Burgersfort rocks are smaller-grained than those from the Jagdlust section, characterized by steeper CSDs with higher intercept values, which is attributed to faster cooling in the Burgersfort region allowing less time for post-nucleation crystal growth and later recrystallization to occur. It is clear that Bushveld "cumulus" textures, and in layered intrusions in general (e.g., McBirney and Hunter 1995), are more a function of post-nucleation compaction, recrystallization and cooling history and only indirectly preserve any information of the original precipitated mineral grain size or shape.

Acknowledgements This work was supported by NSF grants EAR 02-06905 and 04-07928. It was improved with reviews by A. R. McBirney, Nathan Chutas and an unnamed reviewer, whose input is very much appreciated.

References

Benn K, Allard B (1989) Preferred mineral orientations related to magmatic flow in ophiolite layered gabbros. J Petrol 30:925–946
Boorman S, Boudreau A, Kruger FJ (2004) The lower zone—critical zone transition of the Bushveld Complex: a quantitative textural study. J Petrol 45:1209–1235
Boudreau AE (1999) PELE—a version of the MELTS software program for the PC platform. Comput Geosci 25:201–203
Cameron EN (1978) The lower zone of the eastern Bushveld Complex in the Olifants River trough. J Petrol 19:437–462
Eales HV, Cawthorn RG (1996) The Bushveld Complex. In: Cawthorn RG (ed) Layered Intrusions. Elsevier, Amsterdam, pp 181–229
Eales HV, Botha WJ, Hattingh PJ, de Klerk WJ, Maier WD, Odgers ATR (1993) The mafic rock of the Bushveld Complex: a review of emplacement and crystallization history, and mineralization, in the light of recent data. J Afr Earth Sci 16:21–142
Faul UH, Scott D (2006) Grain growth in partially molten olivine aggregates. Contrib Mineral Petrol 151:101–111
Gough DI, van Niekerk CB (1959) A study of the palaeomagnetism of the Bushveld Complex. Phil Mag 14:126–134
Harvey PK, Laxton RR (1980) The estimation of finite strain from the orientation distribution of passively deformed linear markers; eigenvalue relationships. Tectonophysics 70:285–307
Hatton CJ, von Gruenewaldt G (1987) The geologic setting and petrogenesis of the Bushveld chromitite layers. In: Stowe CW (ed) Evolution of chromium ore fields. pp 109–143
Higgins MD (1998) Origin of anorthosite by textural coarsening: quantitative measurements of a natural sequence of textural development. J Petrol 39:1307–1323
Higgins MD (2000) Measurement of crystal size distributions. Am Mineral 85:1105–1116
Higgins MD (2002a) Closure in crystal size distributions (CSD), verification of CSD calculations and the significance of CSD fans. Am Mineral 87:171–175
Higgins MD (2002b) A crystal size-distribution study of the Kiglapait layered mafic intrusion, Labrador, Canada: evidence for textural coarsening. Contrib Mineral Petrol 144:314–330
Hunter RH (1987). Textural equilibrium in layered igneous rocks. In: Parson I (ed) Origins of igneous layering. Reidel, Dordrecht, pp 473–503
Karato SI (1989) Grain growth kinetics in olivine aggregates. Techtonophysics 168:255–273
Klein EM, Langmuir CH, Staudigel H (1991) Geochemistry of basalts from the southeast Indian Ridge, 115 E–138 E. J Geophys Res 96:2089–2107
Kruger FJ (2005) Filling the Bushveld Complex magma chamber: lateral expansion, roof and floor interaction, Magmatic unconformities, and the formation of giant chrmite, PGE and Ti_V magnetite deposits. Mineralium Deposita 40:451–472
Maaloe S (1976) The zoned plagioclase of the Skaergaard intrusion, East Greenland. J Petrol 17:398–419
Marsh BD (1998) On the interpretation of crystal size distributions in magmatic systems. J Petrol 39:553–599
Mathison CI (1987) Pyroxene oikocrysts in troctolitic cumulates—evidence for supercooled crystallization and post-cumulus modification. Contrib Mineral Petrol 97:228–236
McBirney AR, Hunter RH (1995) The cumulate paradigm reconsidered. J Geol 103:114–122
Meurer WP, Boudreau AE (1998a) Compaction of igneous cumulates part II: compaction and the development of igneous foliations. J Geol 106:293–304

Meurer WP, Boudreau AE (1998b) Compaction of igneous cumulates part I: geochemical consequences for cumulates and liquid fractionation trends. J Geol 106:281–292
Nichols SJ, Mackwell SJ (1991) Grain growth in porous olivine aggregates. Phys Chem Miner 18:269–278
Shirley DN (1986) Compaction of igneous cumulates. J Geol 94:795–809
Walraven F (1986) 1:250,000 Geological series map 2430 (Pilgrim's Rest). Republic of South Africa Geologic Survey
Walraven F, Armstrong RA, Kruger FJ (1990) A chronostratigraphic framework for the north-central Kaapvaal Craton, the Bushveld Complex and Vredefort structure. Tectonophysics 171:23–48
Waters C, Boudreau AE (1996) A re-evaluation of crystal size distributions in chromite cumulates. Am Mineral 81:1452–1459